European Journal of
**Immunology**

## Molecular immunology and signaling

## Short Communication

# MALT1 protease function in regulatory T cells induces MYC activity to promote mitochondrial function and cellular expansion

*Marc Rosenbaum[1,2], Theresa Schnalzger[1,2], Thomas Engleitner[2,3], Christin Weiß[1,2], Ritu Mishra[1,2], Cora Mibus[1,2], Theresa Mitterer[1,2], Roland Rad[2,3,4] and Jürgen Ruland[1,2,4,5]*

[1] School of Medicine, Institute of Clinical Chemistry and PathobiochemistryTechnical University of Munich, Munich, Germany
[2] TranslaTUM, Center for Translational Cancer Research, Technical University of Munich, Munich, Germany
[3] School of Medicine, Institute of Molecular Oncology and Functional GenomicsTechnical University of Munich, Munich, Germany
[4] German Cancer Consortium (DKTK), Heidelberg, Germany
[5] German Center for Infection Research (DZIF), Partner Site Munich, Munich, Germany

Regulatory T cells (Tregs) are essential for the inhibition of immunity and the maintenance of tissue homeostasis. Signals from the T-cell antigen receptor (TCR) are critical for early Treg development, their expansion, and inhibitory activity. Although TCR-engaged activation of the paracaspase MALT1 is important for these Treg activities, the MALT1 effector pathways in Tregs remain ill-defined. Here, we demonstrate that MALT1 protease activity controls the TCR-induced upregulation of the transcription factor MYC and the subsequent expression of MYC target genes in Tregs. These mechanisms are important for Treg-intrinsic mitochondrial function, optimal respiratory capacity, and homeostatic Treg proliferation. Consistently, conditional deletion of *Myc* in Tregs results similar to MALT1 inactivation in a lethal autoimmune inflammatory syndrome. Together, these results identify a MALT1 protease-mediated link between TCR signaling in Tregs and MYC control that coordinates metabolism and Treg expansion for the maintenance of immune homeostasis.

Additional supporting information may be found online in the Supporting Information section at the end of the article.

## Introduction

CD4$^+$Foxp3$^+$ regulatory T cells (Tregs) are crucial for the maintenance of immune homeostasis and for the prevention of

immunopathology. However, Tregs are also frequently recruited into tumor microenvironments where their suppressive function can restrict effective antitumor immune responses [1]. Thus, there is a strong interest in modulating the function of Tregs for therapeutic purposes [2].

Signals from the T-cell antigen receptor (TCR) are critical for the development of Tregs in the thymus and periphery and

*Correspondence:* Dr. Jürgen Ruland
e-mail: j.ruland@tum.de
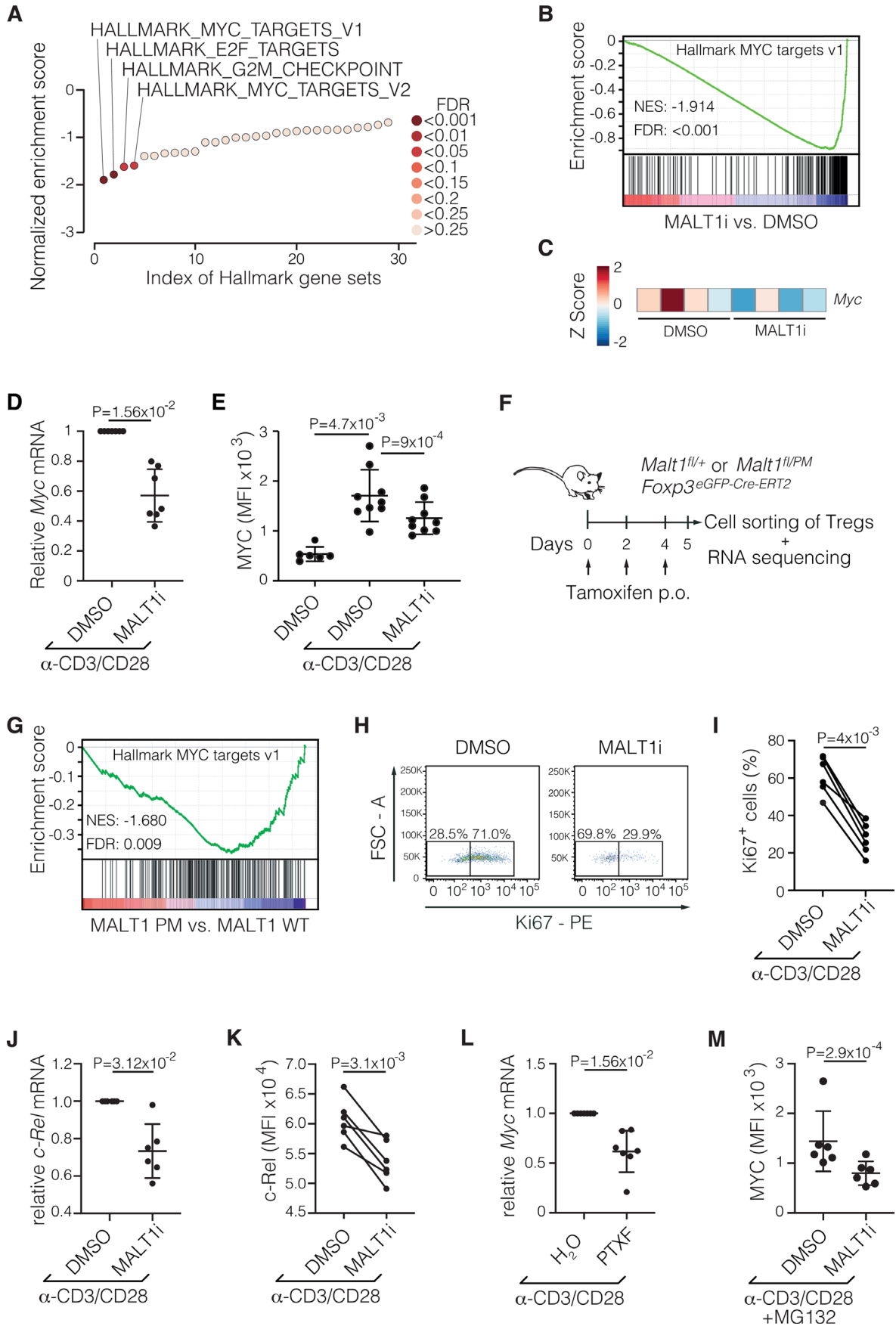
for their subsequent expansion and differentiation into immune suppressive effector Tregs (eTregs) [3, 4]. Here, TCR-induced activation of the CARD11-BCL10-MALT1 (CBM) signalosome is particularly important [5–8] given that loss-of-function mutations in CARD11, BCL10, or MALT1 in both mice and humans result in severe Treg deficiencies [9]. Upon TCR proximal signaling, CBM complexes form large signalosomes that serve as scaffolds for the recruitment of ubiquitin regulators, such as TRAF6 for canonical NF-κB activation [10]. In addition, MALT1 functions as a proteolytic paracaspase that can cleave, at least in conventional T (Tconv) cells, a series of substrates, such as A20, CYLD, HOIL1, and RELB, to finetune the NF-κB response as well as RNA stability regulators, such as Roquins 1/2 and Regnase-1, to provide an additional layer of T-cell control [11]. Given that this activity of MALT1 can be inhibited with small molecule inhibitors, MALT1 is a clinically explored drug target for immune intervention [12–14].

In Tregs, the proteolytic activity of MALT1 controls early Treg differentiation and mature Treg function given that gene-targeted knock-in mice that carry an inactivating point mutation in the MALT1 proteolytic domain (MALT1 paracaspase mutant [PM] mice) exhibit severe reductions in peripheral Foxp3$^+$ Tregs [15–18]. Within established Tregs, the proteolytic activity of MALT1 mediates immunosuppressive activity in peripheral tissues [5–7], demonstrating that the proteolytic function of MALT1 is crucial for Treg-controlled immune homeostasis. Importantly, pharmacological targeting of the MALT1 protease by small molecules can release Treg-inhibitory effects in tumor microenvironments and thereby augment antitumor immunity in vivo [5, 6]. Nevertheless, the MALT1 protease-controlled effector pathways in Tregs that maintain immune homeostasis are unknown.

Here, we report that MALT1 protease activity in Tregs strongly promotes the TCR-induced upregulation of MYC, which is critical for homeostatic expansion of Tregs. Using a genetic approach with conditional *Myc*-deficient mice or pharmacologic intervention with MYC activity, we further demonstrate that MYC is critical for mitochondrial function and Treg expansion and for the prevention of immunopathology. Consistent with the key role of the MALT1 protease in MYC regulation, MALT1 activity promotes the expression of MYC-controlled mitochondrial regulators and mitochondrial activity. Thus, our study reveals a previously unrecognized link between TCR-induced MALT1 activity and MYC regulation for Treg-controlled immune homeostasis.

## Results and discussion

### MALT1 protease activity controls the TCR-induced upregulation of MYC

To investigate the mechanisms by which MALT1 proteolytic activity affects the function of Tregs, we FACS-purified naïve CD4$^+$EYFP$^+$CD62L$^+$ resting Tregs (rTregs) from *Rosa26$^{LSL-EYFP}$;Foxp3$^{IRES-Cre}$* (FIC) mice, which express an EYFP reporter upon Cre recombinase-mediated deletion of the *loxP*-flanked STOP cassette (LSL) selectively in FoxP3$^+$ Treg cells [19, 20]. Subsequently, we stimulated these rTregs via their TCR and the CD28 coreceptor with or without acute blockage of MALT1 paracaspase activity using the MALT1 inhibitor (MALT1i) mepazine [21]. Sixteen hours later, we performed RNA sequencing analysis and compared the gene expression signatures of MALT1-inhibited TCR/CD28-stimulated rTregs to dimethyl sulfoxide (DMSO)-treated control cells. Altogether, we identified four gene sets from the hallmark gene set collection of the Molecular Signatures Database with significantly less expression in MALT1i-treated Tregs compared to the control. Intriguingly, among these four hallmark gene sets were the two MYC target gene sets v1 and v2 (Fig. 1A). The MYC target gene set v1 represented the top differentially expressed gene set with the highest normalized enrichment score in the entire gene set enrichment analysis (Fig. 1B). At the individual gene level, the expression of *Myc* mRNA itself was also significantly increased in stimulated noninhibited compared with MALT1-inhibited Tregs (Fig. 1C and D and Supporting Information Fig. 1A). Furthermore, TCR/CD28 triggering of control rTregs increased intracellular MYC protein expression, this upregulation of MYC was significantly impaired in MALT1i-treated rTregs (Fig. 1E). Thus, TCR/CD28 triggering in primary naïve rTregs induces *Myc* mRNA and MYC protein expression in a MALT1 protease-dependent manner, which drives MYC v1 and v2 target gene expression.

**Figure 1.** TCR-induced upregulation of MYC requires MALT1 protease activity. Gene set enrichment analysis (A) and enrichment plot of hallmark MYC targets v1 (B) in sorted splenic CD4$^+$EYFP$^+$CD62L$^+$ rTregs from *Rosa26$^{LSL-EYFP}$*;FIC mice after 16 h of treatment with the MALT1 inhibitor (MALT1i) mepazine (5 µM) versus DMSO as a control and concurrent anti-CD3/28 bead stimulation. NES: normalized enrichment score; FDR: false discovery rate. (C) Heat map of *Myc* expression from RNAseq data shown in (A). (D) qRT-PCR analysis of *Myc* mRNA expression in rTregs sorted and treated as noted in (A). Statistical differences were assessed using a Wilcoxon signed-rank test. (E) Median fluorescence intensity (MFI) of MYC in splenic rTregs sorted and stimulated as noted in (A). Corresponding biological replicates between the indicated conditions were treated as repeated measures, and significant differences between conditions were assessed by mixed-effects analysis with Geisser–Greenhouse correction and Tukey's multiple comparisons test. (F) Schematic representation of the acute genetic deletion of the MALT1 paracaspase function in Tregs. (G) Enrichment plot of hallmark MYC targets v1 in sorted peripheral CD4$^+$EGFP$^+$ Tregs from male *Malt1$^{fl/PM}$;Foxp3$^{eGFP-Cre-ERT2}$* mice (MALT1 PM) and *Malt1$^{fl/+}$;Foxp3$^{eGFP-Cre-ERT2}$* control animals (MALT1 WT) following tamoxifen administration. (H and I) Representative FACS experiment (H) and frequencies (I) of Ki67$^+$ proliferating cells in sorted splenic CD4$^+$EYFP$^+$CD62L$^+$ rTregs from *Rosa26$^{LSL-EYFP}$*;FIC mice after 3 days under the stimulation conditions of (A). (J and K) qRT-PCR analysis of *c-Rel* mRNA expression (J) and flow cytometric analysis of c-Rel protein levels (K) in rTregs sorted and treated as noted in (A). (L) Relative *Myc* mRNA levels in rTregs sorted and stimulated as in (A) in the presence of the c-Rel inhibitor pentoxifyllin (PTXF, 500 µg mL$^{-1}$) or DMSO as a control. (M) MFI of MYC in CD4$^+$EYFP$^+$-gated rTregs sorted as in (A) and stimulated for 16 h with anti-CD3 and anti-CD28-coated beads and MG132 (5 µM) in the presence of the MALT1i mepazine (5 µM) or DMSO as a control. Bars in (D), (E), (J), (L), and (M) show the mean ± SD, and statistical significance was assessed using a two-tailed ratio-paired *t* test (I, K, and M) or a Wilcoxon signed-rank test (D, J, and L). Data are cumulative from *n* = 2 (E, K, and M) or *n* = 3 (D, I, J, and L) independent experiments, or representative of *n* = 3 independent experiments with a total of *n* = 6 biological replicates (H).
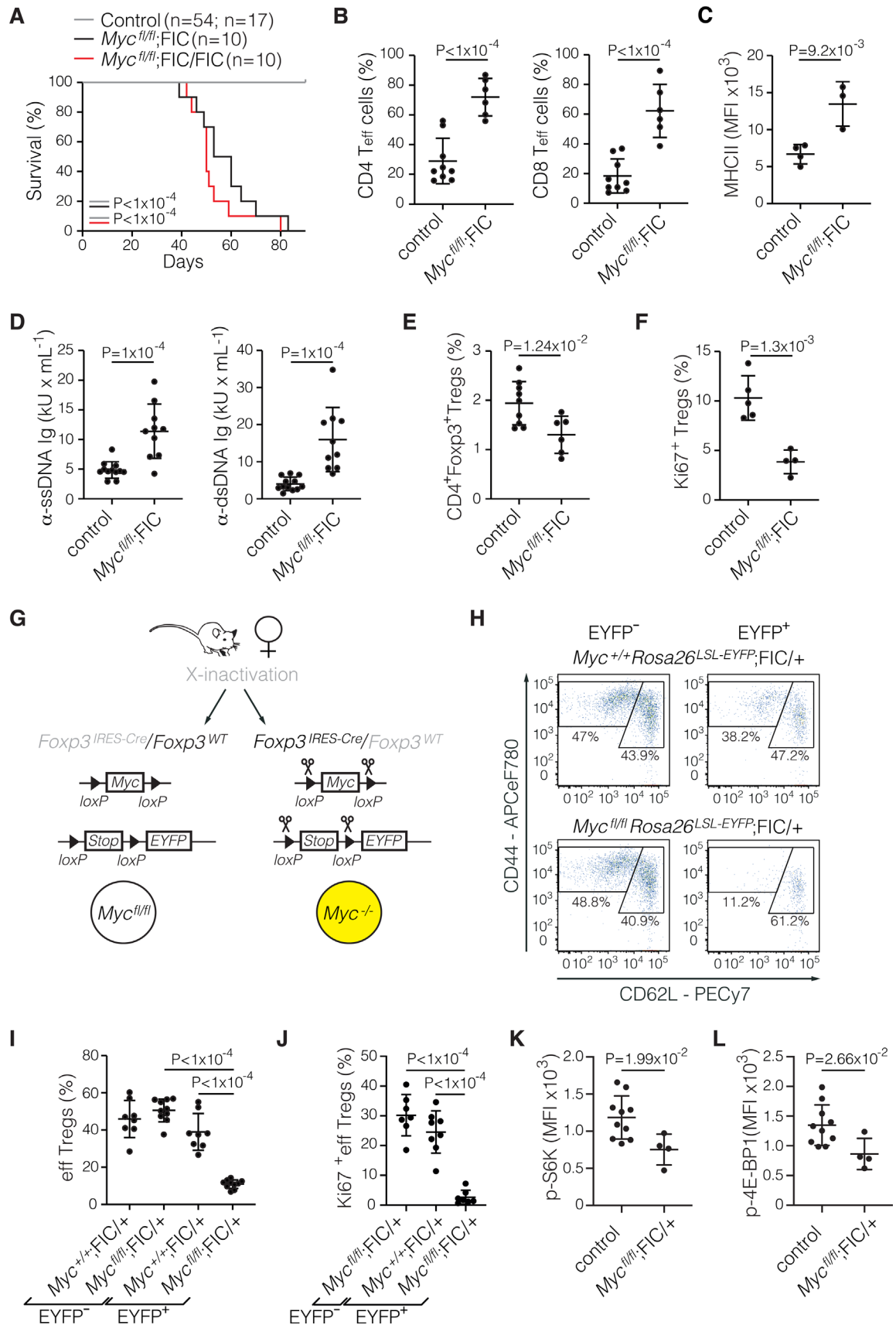
In order to exclude off-target effects by the pharmacologic MALT1 inhibitor, we additionally employed a genetic approach and intercrossed $Malt1^{fl/PM}$ mice with $Foxp3^{eGFP-Cre-ERT2}$ animals, which express a tamoxifen-responsive Cre-ER$^{T2}$ recombinase from the $Foxp3$ gene locus. We then utilized $Malt1^{fl/PM};Foxp3^{eGFP-Cre-ERT2}$ mice or $Malt1^{fl/+};Foxp3^{eGFP-Cre-ERT2}$ control offspring animals to acutely delete the floxed $Malt1$ allele by tamoxifen administration (Fig. 1F), retaining the $Malt1^{PM}$ allele, which is selectively paracaspase defective. Consistent with our pharmacological data, the acute genetic Treg-intrinsic ablation of the MALT1 paracaspase function resulted also in a significant decrease in the expression of the hallmark MYC target gene set v1 (Fig. 1G).

In addition to hallmark MYC targets, the other gene sets with impaired expression in MALT1i-treated and genetically protease-inhibited rTregs are the hallmark E2F target gene set and the hallmark G2M checkpoint gene set (Fig. 1A, Supporting Information Fig. 1B and C ), which are both linked to cellular proliferation and are also controlled by MYC in many different cell types [22].

Based on these intriguing results from gene expression analysis, we next investigated the functional roles of MALT1 proteolytic activity on the proliferation of Tregs. Therefore, we stimulated FACS-isolated rTregs in the presence or absence of MALT1i with anti-CD3/28-coated beads and measured intracellular Ki67 expression as a marker for cellular proliferation. Consistent with the impaired expression of MYC target programs as well as hallmark E2F targets and hallmark G2M checkpoint genes, acute MALT1 inhibition also resulted in reduced proliferation of TCR/CD28-stimulated rTregs (Fig. 1H and I). Thus, MALT1 protease activity regulates MYC expression and is required for the efficient expansion of TCR/CD28-triggered Tregs.

Previously, it has been demonstrated that c-Rel can in principle transactivate $Myc$ expression [23]. To explore a putative link between MALT1, c-Rel, and MYC in Tregs, we next analyzed $c$-$Rel$ mRNA and protein levels in MALT1-inhibited rTregs. Intriguingly, upon TCR stimulation, c-Rel expression was significantly impaired by MALTi treatment (Fig. 1J and K). Next, we blocked c-Rel induction or activity in TCR/CD28-stimulated rTregs with the chemical compounds pentoxifyllin (PTXF) or IT-603, which inhibit anti-CD3-induced c-Rel expression and DNA binding of c-Rel, respectively [24–26]. Both inhibitors significantly decreased

the transcription of $Myc$ (Fig. 1L and Supporting Information Fig. 1D), indicating together that the MALT1 protease controls $Myc$ mRNA at least in part via c-Rel. To study whether MALT1 could additionally regulate the proteasomal degradation of MYC, we also treated the cells with the proteasomal inhibitor MG132. However, this treatment did not mitigate the effects of the MALT1i treatment on MYC protein levels in sorted TCR/CD28-stimulated Tregs (Fig. 1M).

## Myc is required for Treg expansion and prevents fatal autoimmune disease

To directly analyze the biological functions of $Myc$ in Tregs in vivo, we selectively deleted $Myc$ in Tregs by crossing $Myc^{fl/fl}$ mice [27] with FIC animals, which express Cre recombinase under the control of the X-chromosomally located $Foxp3$ locus [19] (Supporting Information Fig. 2A and B). Both male $Myc^{fl/fl};$FIC and female $Myc^{fl/fl};$FIC/FIC mice developed a lethal autoinflammatory syndrome with splenomegaly and lymphadenopathy, requiring euthanasia of the animals at approximately 57 days of age (Fig. 2A and Supporting Information Fig. 2C). The wasting disease is characterized by a massive accumulation of CD4$^+$ and CD8$^+$ CD44$^{hi}$CD62L$^{lo}$ effector T lymphocytes and pathological B-cell activation with autoantibody production (Fig. 2B–D, Supporting Information Fig. 2D and E). We observed a significant reduction in the percentage of CD4$^+$Foxp3$^+$ Tregs (Fig. 2E), which was accompanied by a marked decrease in the frequency of Ki67$^+$ proliferating cells within this population (Fig. 2F), although the total number of CD4$^+$Foxp3$^+$ Tregs were similar (Supporting Information Fig. 2F). These data indicate that Tregs cannot counteract the massive accumulation and activation of Tconv eff cells. The overall phenotype of these animals is similar to the phenotype of Treg-specific MALT1 paracaspase mutant ($Malt1^{fl/PM};$FIC) mice [5, 7] and consistent with a recently published independent study of $Myc$ in Tregs [28], indicating that MALT1-mediated $Myc$ control is important for the maintenance of immune homeostasis.

To further extend these findings and to specifically address the Treg-intrinsic functions of $Myc$ without confounding effects of inflammation, we analyzed female $Myc^{fl/fl};$FIC/+ mice. Due

**Figure 2.** $Myc$ prevents a fatal autoimmune disease and is essential for the expansion of Tregs. (A) Survival curves of male $Myc^{fl/fl};$FIC ($n = 10$) and female $Myc^{fl/fl};$FIC/FIC ($n = 10$) mice compared to male $Myc^{+/+};$FIC and $Myc^{+/fl};$FIC ($n = 54$) as well as female $Myc^{+/+};$FIC/FIC and $Myc^{+/fl};$FIC/FIC ($n = 17$) control mice. Statistical significance between survival curves was calculated using a log-rank (Mantel–Cox) test. (B) Frequency of CD4$^+$Foxp3$^-$ and CD8$^+$ CD44$^{hi}$CD62L$^{lo}$ effector (eff) T cells in the spleens of diseased male $Myc^{fl/fl};$FIC in comparison to control mice ($Myc^{fl/fl}$, $Myc^{+/+};$FIC, $Myc^{+/fl};$FIC) as measured by FACS. (C) Median fluorescence intensity (MFI) of cell surface MHCII on CD19$^+$-gated splenic B cells of diseased male $Myc^{fl/fl};$FIC and control mice ($Myc^{fl/fl}$, $Myc^{+/+};$FIC). (D) Immunoglobulin levels of anti-ssDNA and anti-dsDNA in the sera of diseased male $Myc^{fl/fl};$FIC mice compared to control mice ($Myc^{fl/fl}$, $Myc^{+/fl};$FIC, $Myc^{+/fl};$FIC). (E and F) Frequency of viable CD4$^+$Foxp3$^+$ Tregs (E) and Ki67$^+$ proliferating cells (F) within the splenic viable CD4$^+$Foxp3$^+$ Treg population of diseased male $Myc^{fl/fl};$FIC versus control mice ($Myc^{fl/fl}$, $Myc^{+/+};$FIC). (G) Schematic illustration of Tregs from $Myc^{fl/fl};Rosa26^{LSL-EYFP};$FIC/+ mice. (H and I) FACS profiles (H) and frequencies (I) to detect either EYFP$^-$ (left) or EYFP$^+$ (right) CD62L$^{hi}$ rTregs and CD44$^{hi}$CD62L$^{lo}$ eff Tregs in the viable splenic CD4$^+$Foxp3$^+$ Treg population from female $Myc^{+/l+};Rosa26^{LSL-EYFP};$FIC/+ and $Myc^{fl/fl};Rosa26^{LSL-EYFP};$FIC/+ mice. Plots are representative of ≥8 mice each. (J) Frequencies of EYFP$^-$ and EYFP$^+$-gated Ki67$^+$-proliferating cells in the viable splenic CD4$^+$Foxp3$^+$CD44$^{hi}$CD62L$^{lo}$ eff Treg population of female $Myc^{+/l+};Rosa26^{LSL-EYFP};$FIC/+ and $Myc^{fl/fl};Rosa26^{LSL-EYFP};$FIC/+ mice. (K and L) MFI of phospho (p)-S6 Kinase (S6K) (K) and p-4E-BP1 (L) in CD4$^+$EYFP$^+$-gated Tregs from adult female $Myc^{fl/fl};Rosa26^{LSL-EYFP};$FIC/+ mice in comparison to $Myc^{+/+};Rosa26^{LSL-EYFP};$FIC/+ and $Myc^{+/+};Rosa26^{LSL-EYFP};$FIC control mice. Statistical significance was assessed using a two-tailed unpaired Student's t test (B–F, K, and L) or a standard one-way ANOVA combined with Tukey's multiple comparisons test (I and J); bars represent the mean ± SD. Data are cumulative from five (B), two (C, K, and L), and three (E, F, I, and J) independent experiments.

to random X inactivation and FIC-mediated Cre expression in only half of the Treg population [29], female $Myc^{fl/fl}$;FIC/+ mice exhibit a mosaic Treg population and thus carry $Myc$-expressing and $Myc$-deficient Tregs (Fig. 2G). Given that we did not observe any significant differences in the activation of Tconv and B cells in female $Myc^{fl/fl}$;FIC/+ mice (Supporting Information Fig. 3A–C), the MYC-expressing ($Myc^{fl/fl}$;+) population is sufficient to maintain immune homeostasis and allows the study of MYC-deficient ($Myc^{-/-}$;FIC) Tregs in a noninflammatory environment. To distinguish MYC-deficient from MYC-expressing Tregs within female $Myc^{fl/fl}$;FIC/+ mice, we additionally crossed a $Rosa26^{LSL-EYFP}$ reporter allele [20] into compound mutant animals, which allowed monitoring of Cre recombinase activity within individual cells due to EYFP expression after deletion of the LSL cassette (Fig. 2G). Under these noninflamed conditions, the frequency of EYFP+ $Myc^{-/-}$;FIC eTregs was reduced compared to that of EYFP− $Myc^{fl/fl}$;+ eTregs from $Myc^{fl/fl}$;FIC/+ mice or EYFP+ $Myc^{+/+}$;FIC eTregs from $Myc^{+/+}$;FIC/+ control mice (Fig. 2H and I). Notably, the frequency of Ki67+-proliferating cells in the EYFP+ $Myc$-deficient eTreg population was also significantly decreased compared to EYFP− eTregs from $Myc^{fl/fl}$;FIC/+ mice or EYFP+ eTregs from $Myc^{+/+}$;FIC/+ control mice (Fig. 2J), indicating that the presence of $Myc$ is critical for eTreg proliferation and the establishment of a proper eTreg compartment to maintain immune homeostasis. In line with a critical role of $Myc$ in Treg expansion, we also observed a significantly reduced proliferation of TCR/CD28-stimulated rTregs upon $Myc$ deficiency (Supporting Information Fig. 3D). MALT1i treatment did not further affect the proliferation of these $Myc$-deficient stimulated rTregs (Supporting Information Fig. 3D), indicating no additional MALT1 protease-dependent proliferative effects for Treg expansion. Since MYC can interact with the mTOR pathway [30, 31], we also probed mTORC1 signaling in Tregs from female $Myc^{fl/fl}$;FIC/+ mice. The phosphorylation of S6 kinase, S6, and 4E-BP1 were all significantly decreased in $Myc$-deficient CD4+EYFP+ Tregs compared to their $Myc$-proficient control cells (Fig. 2K and 2L and Supporting Information Fig. 3E). Thus, MYC and mTORC1 pathway cross-talk in Tregs and defective mTORC1 signaling presumably contributes to the impairment of $Myc$-deficient Tregs.

### The MALT1-MYC axis regulates mitochondrial function in Tregs

MYC is a central transcription factor controlling metabolic programs in multiple cell types, including Tconv cells [32]. Here, MYC activity is critical to provide sufficient energy and to supply building blocks for clonal expansion and effector function upon activation [30]. Because Tregs preferentially rely on mitochondrial metabolism for their proliferation and survival [33–35] and given that MYC can control oxidative phosphorylation [36], we next studied the putative role of MYC in the mitochondrial function of Tregs. To this end, we isolated Tregs from WT animals to obtain sufficient numbers of Tregs for Seahorse mito-

chondrial stress test analysis and acutely blocked MYC activity during TCR/CD28 stimulation with the MYC inhibitor 10058-F4, which disrupts the MYC-MAX interaction [37]. In the mitochondrial stress test, we detected a decrease in maximal respiration and a reduced spare respiratory capacity in MYC-inhibited cells compared to control cells (Fig. 3A–C). These respiratory deficiencies were accompanied by a significantly reduced mass of active mitochondria, which is indicated by reduced labeling of the cells with MitoTracker Deep Red stain (Fig. 3D). Similar defects were previously observed in the mitochondria of MYC-deficient rats and murine fibroblasts, which exhibit severe structural defects and functional deficits in electron transport chain complexes [38, 39]. Because MALT1 controls MYC in Tregs, we next investigated whether MALT1 inhibition would also affect their mitochondrial function. Therefore, we stimulated rTregs from $Rosa26^{LSL-EYFP}$;FIC mice in the presence or absence of MALT1i with anti-CD3/CD28-coated beads and first examined the expression of previously established MYC-regulated mitochondrial factors [40]. Interestingly, MALT1 protease inhibition significantly impaired mRNA expression of the electron transport chain component $Cox5a$, the mitochondrial import receptor subunit $Tomm70a$ and the mitochondrial chaperonins $Hspd1$ and $Hspe1$ (Fig. 3E). Next, we studied mitochondrial numbers and activities in MALT1-inhibited rTregs after TCR/CD28 stimulation. Using MitoTracker Deep Red staining and confocal microscopy, we also detected significantly reduced numbers of mitochondria in MALT1i-treated stimulated rTregs compared to DMSO-treated control cells (Fig. 3F and G). Moreover, using extracellular flux analysis, we detected that MALT1i-treated TCR/CD28-stimulated Tregs exhibited a significant reduction in maximal respiration and spare respiratory capacity that was similar to MYC-inhibited Tregs compared to DMSO-treated control cells (Fig. 3H–J).

To test whether these effects of MALT1 are specific to Tregs, we also treated TCR/CD28-stimulated naïve CD4+ Tconv cells with MALT1i. Interestingly, the same MALT1i treatment as in Tregs did not affect the expression of $Myc$ mRNA and MYC-regulated mitochondrial factors in naïve CD4+ Tconv cells, nor did it alter mitochondrial respiration (Supporting Information Fig. 4A–D). Thus, MALT1 protease activity regulates MYC and mitochondrial function in a Treg-specific manner.

### Concluding remarks

Together, our data demonstrate that MALT1 protease activity in Tregs couples TCR signaling to the activation of the transcription factor MYC to induce MYC-dependent gene transcription. This pathway is important for Treg mitochondrial metabolism and optimal respiratory capacity to orchestrate Treg proliferation for the maintenance of immune homeostasis. In line with this hypothesis, conditional deficiency of $Myc$ in FoxP3+ Tregs results in a fatal autoimmune disease, which is consistent with an independent study [28] that was published while our manuscript was in preparation. In addition, the MALT1-dependent MYC pathway is
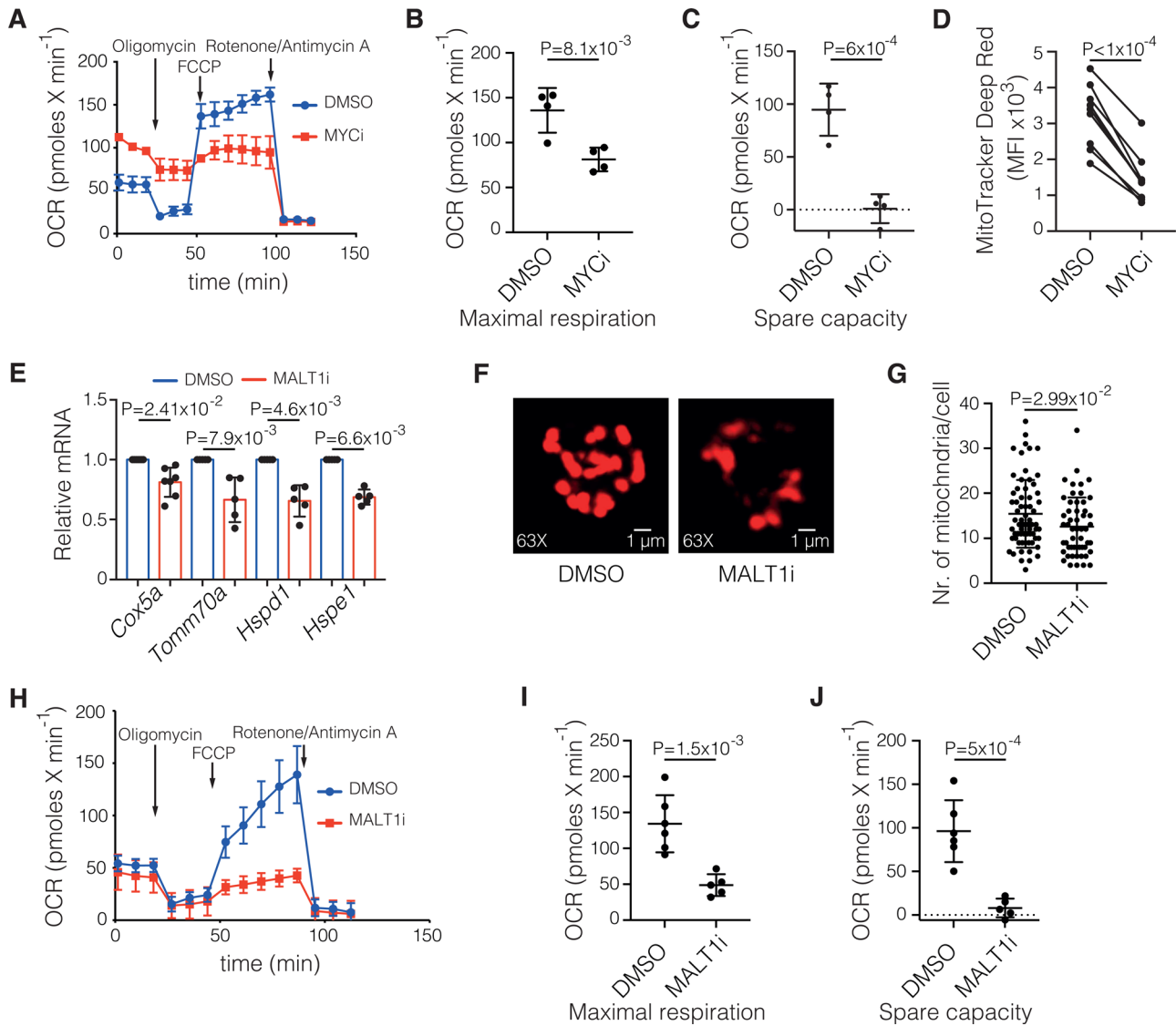
**Figure 3.** The MYC-MALT1 axis controls mitochondrial function in Tregs. (A) Seahorse Mito stress test of sorted CD4$^+$CD25$^+$CD45RB$^{lo}$ Tregs from C57BL/6N WT mice after 16-h stimulation using anti-CD3/28 beads in the presence of the MYC inhibitor (MYCi) 10058-F4 (64 $\mu$M) or DMSO as a control. Data are representative of $n = 2$ independent experiments with duplicate measurements per condition. (OCR) Oxygen consumption rate. (B) Maximal respiration calculated by subtracting the nonmitochondrial oxygen consumption rate (OCR) under rotenone/antimycin A ($t = 121$ min) from the OCR under FCCP ($t = 96$ min) as shown in (A). (C) Spare capacity calculated by subtracting the basal OCR ($t = 10$ min) from the maximal OCR under FCCP ($t = 96$ min) as shown in (A). (D) Median fluorescence intensity (MFI) of MitoTracker Deep Red after labeling sorted CD4$^+$EYFP$^+$CD62L$^+$ rTregs from *Rosa26$^{LSL-EYFP}$*;FIC mice treated as noted in (A). (E) Relative mRNA expression of the indicated genes as analyzed by qRT-PCR in sorted splenic CD4$^+$EYFP$^+$ CD62L$^+$ rTregs from *Rosa26$^{LSL-EYFP}$*;FIC mice after 16 h of stimulation using anti-CD3/28 beads in the presence of MALT1i mepazine (5 $\mu$M) or DMSO as a control. (F and G) Confocal microscopic analysis (F) with a 63× magnification of sorted CD4$^+$EYFP$^+$CD62L$^+$ rTregs from *Rosa26$^{LSL-EYFP}$*;FIC mice treated as in (E) and subsequent MitoTracker Deep Red labeling to determine the number (Nr.) of mitochondria (G). (H) Seahorse Mito stress test of sorted CD4$^+$CD25$^+$CD45RB$^{lo}$ Tregs from C57BL/6N WT mice treated as noted in (E). Data are representative of $n = 2$ independent experiments with $n \geq 2$ measurements per condition. (I) Maximal respiration calculated by subtracting the nonmitochondrial oxygen OCR under rotenone/antimycin A ($t = 104$ min) from the OCR under FCCP ($t = 87$ min) as shown in (H). (J) Spare capacity is calculated by subtracting the basal OCR ($t = 10$ min) from the maximal OCR under FCCP ($t = 87$ min) as shown in (H). Bars in (A–C), (E), (G–J) represent the mean ± SD, and statistical significance was assessed using a two-tailed unpaired Student's $t$ test (B, C, G, I, and J), a two-tailed ratio-paired $t$ test or a Kruskal–Wallis test with Dunn's multiple comparisons test (E). Data are cumulative from two (B–E, G, I, and J) and three (*Cox5a* in E) independent experiments.

critical for the homeostatic expansion of Tregs under noninflamed conditions. Although MALT1 protease activity can also regulate MYC activity in cell line models of mantle cell lymphoma [41], the MALT1-MYC axis seems to operate and regulate mitochondrial function in a cell type-specific manner. Our data further suggest

that the mechanisms by which MALT1 proteolytic activity controls MYC in Tregs involves c-Rel-dependent *Myc* gene transcription [23]. Additional direct or indirect effects via mRNA stability regulators such as Regnase-1 or Roquin are conceivable, since these are not cleaved in MALT1 paracaspase-mutated Tregs [5].

Because our pharmacological and genetic data indicate a critical function of the MALT1-MYC pathway for Treg-mediated immune suppression and current strategies aim at restricting Treg activity in tumor microenvironments to enhance antitumor immune responses, our results suggest further exploration of the potential function of the Treg-intrinsic MALT1-MYC pathway as a drug target for immuno-oncology.

## Materials and methods

### Mice

All mouse experiments were legally approved by the Government of Upper Bavaria(reference numbers ROB55.2-2532.Vet_02-15-26, ROB55.2-2532.Vet_02-15-207 and ROB 55.2-2532.Vet_02-20-94), and we complied with all relevant ethical regulations for animal testing, research, and euthanasia.

*Foxp3*[IRES-Cre] mice [19], *Rosa26*[LSL-EYFP] mice [20], *Foxp3*[eGFP-Cre-ERT2] mice [42], *Malt1*[fl/PM] mice [5, 15], and *Myc*[fl] mice [27] (ordered from Jackson Laboratory) were bred at the institute's animal care facility under specific pathogen-free conditions and genotyped using the indicated primers (Supporting Information Table 1). The sex of the mice used is indicated in the figure legends. Adult mice aged 6–12 weeks were used for all experiments; littermate controls were used whenever possible.

### *In vivo* tamoxifen treatment

Male *Malt1*[fl/PM];*Foxp3*[eGFP-Cre-ERT2] mice and *Malt1*^{fl/+};*Foxp3*[eGFP-Cre-ERT2] control mice were treated perorally on day 0 with 5 mg tamoxifen (Hexal) in ClinOleic 20% (Baxter). The peroral administration of 5 mg tamoxifen was repeated each second day to delete the floxed allele in newly emerging Tregs until the final analysis on day 5.

### RNA sequencing

Tregs were subjected to live/dead cell staining, and 1000 viable cells per well were sorted into a 96-well PCR plate prefilled with 10 μL of 1X TCL buffer (Qiagen) containing 1% (v v$^{-1}$) β-mercaptoethanol (Sigma-Aldrich). Library preparation for bulk 3′-sequencing of poly(A)-RNA was performed as outlined by Parekh et al. [43]. P5 and P7 sites were exchanged to allow sequencing of the cDNA in read1 and barcodes and Unique Molecular Identifiers (UMIs) in read2 to achieve better cluster recognition. The library was sequenced on the NextSeq 500 platform (Illumina) with 75 cycles for cDNA and 16 cycles for barcodes and UMIs. Raw sequencing data were processed with DropSeq-tools version 1.12 using gene annotations from the Ensembl GRCm38.87 database to generate sample and genewise UMI tables [44]. Downstream analysis was conducted with R v3.4.4 [45] and DESeq2 v1.18.1

[46], or *limma* v3.46.0 [47] in case of the genetic model. Gene set enrichment analysis was performed in the preranked mode using the hallmark gene set collection from the Molecular Signatures Database (MSigDB) v7.4 [48].

### Flow cytometry

Organs were meshed, and erythrocytes were lysed using G-DEXIIb RBC Lysis Buffer (iNtRON Biotechnology). Following live/dead cell staining using a fixable viability dye at 1:1000 dilution (Thermo Fisher or Biolegend) and blocking by anti-CD16/32 clone 93 at 1:300 dilution (Thermo Fisher), surface antigens were stained in PBS/2% FCS with fluorochrome-coupled antibodies (1:400) purchased from Thermo Fisher, BD Biosciences, or BioLegend: anti-CD4 (GK1.5), anti-CD8 (53-6.7), anti-CD19 (1D3), anti-CD25 (PC61.5), anti-CD44 (IM7), anti-CD45RB (C363.16A), anti-CD62L (MEL.14), and anti-MHCII (M5/114.15.2). Subsequently, cells were fixed with 2% formalin for 40 min, permeabilized with 1× perm/wash buffer (Thermo Fisher), and stained with anti-Foxp3 clone (FJK-16s; 1:300), anti-Ki67 (SolA15; 1:500), and anti-c-Rel (sc-71, Santa Cruz Biotechnology; 1:200) or anti-MYC (D84C12, Cell Signaling; 1:100) followed by anti-rabbit IgG-APC (A10931, Thermo Fisher; 1:1000). For Phos-flow experiments, cell viability staining was performed directly in the medium (Biolegend; 1:60) and cells were fixed with 4% formaldehyde (Thermo Fisher) for 10 min. After permeabilization with 100% ice-cold methanol for 30 min at –20°C, Fc blocked-cells were stained in PBS/2% FCS with anti-phospho (p)-4EBP1 (#5536, Cell Signaling; 1:50), anti-p-S6 (#4858, Cell Signaling; 1:50), or anti-p-p70 S6 Kinase (#9234, Cell Signaling; 1:50) for 1 h followed by an anti-rabbit IgG-APC secondary antibody (A10931, Thermo Fisher; 1:2000). Mitochondrial staining was performed for 15 min with 5 nM MitoTracker Deep Red (Thermo Fisher) at 37°C and 5% $CO_2$. For cell sorting, splenic T cells were pre-enriched by a CD4$^+$ T cell isolation kit (Miltenyi).

All cells were acquired on a FACSCanto II or sorted with a FACSAria III (BD Biosciences) followed by data analysis with FlowJo version 9.7.7. We adhered to the "Guidelines for the use of flow cytometry and cell sorting in immunological studies" [49], and the gating strategies used are depicted in Supporting Information Fig. 5.

### Treg culture

Sorted rTregs were plated in RPMI 1640 (Thermo Fisher) supplemented with 10% (v v$^{-1}$) FCS (Capricorn Scientific), 1% (v v$^{-1}$) penicillin-streptomycin-glutamine, 1 mM sodium pyruvate, 10 mM HEPES, 1× Gibco MEM NE-AA, and 56 μM β-mercaptoethanol (Thermo Fisher) into a 96-well U-bottom plate. After 30 min of pretreatment with the MALT1 protease inhibitor mepazine (5 μM, Millipore), the MYC inhibitor 10058-F4 (64 μM, Merck), the c-Rel inhibitors pentoxifyllin (PTXF, 500 μg mL$^{-1}$, Merck) and IT-603 (20 μM, Merck), or the proteasome inhibitor MG132 (5 μM, Merck), cells were stimulated with Dynabeads

Mouse T-Activator CD3/CD28 (Thermo Fisher) for 16 h or 3 days at 37°C and 5% $CO_2$.

## qRT-PCR

Total RNA was isolated using the RNeasy Plus Micro kit (Qiagen), reverse transcribed with qScript cDNA Super Mix (Quantabio), and analyzed with No ROX SYBR MasterMix blue dTTP (Takyon) and respective primers (Supporting Information Table S1) in a Light Cycler 480II (Roche). Data were analyzed according to the ddCt method.

## Immunoblot

Washed cells were resuspended in RIPA buffer (50 mM Tris/Cl pH 8.0, 150 mM NaCl, 1.0% (v v$^{-1}$) NP-40, 0.5% (w v$^{-1}$) deoxycholate) supplemented with protease inhibitor cocktail (Calbiochem), 10 mM NaF, and 4 mM $Na_3VO_4$. The cell lysate was centrifuged, and the supernatant was subjected to WES immunoblotting (ProteinSimple) according to the manufacturer's protocol using the following polyclonal antibodies: anti-MYC (#9402, Cell Signaling; 1:20) and anti-β-Actin (#4967, Cell Signaling; 1:100).

## ELISA

Immunoglobulins against autoantigens in mouse sera were measured using autoantibody ELISA kits (Alpha Diagnostic International).

## Metabolic assay

Tregs ($2 \times 10^5$) were plated into a CellTak (22.4 µg x mL$^{-1}$; Fisher Scientific)-coated Seahorse XF96 Cell Culture Microplate in Seahorse XF RPMI medium pH 7.4 (Agilent Technologies) supplemented with 25 mM glucose (Merck), 2 mM L-glutamine (Thermo Fisher), and 1 mM sodium pyruvate (Thermo Fisher) and incubated for 30 min in a non-$CO_2$ incubator. OCR was measured in a Seahorse XF96 extracellular flux analyzer with sequential injection of a final concentration of 1 µM oligomycin, 0.5 µM FCCP, and 0.1 nM rotenone/0.5 µM antimycin A (Merck).

## Confocal microscopy

Tregs were labeled for 15 min with 30 nM MitoTracker Deep Red (Thermo Fisher) at 37°C and 5% $CO_2$, resuspended in Live Cell Imaging solution (Thermo Fisher) supplemented with 11.11 mM D-Glucose (Merck), and analyzed on a Leica DMi8 with an HC PL APO CS2 63x/1.20 water objective (Leica Microsystems). Total numbers of mitochondria per cell were determined using Imaris

viewer software version 9.5 (Bitplane) and generating a surface fitting the mitochondrial structure for all cells within one experiment.

## Quantification and statistical analysis

Statistical tests for $\alpha = 0.05$ were performed with GraphPad Prism 7.0c software and are indicated in each figure legend. The median fluorescence intensity (MFI) was calculated using FlowJo version 9.7.7.

**Author contributions:** M.R. and J.R. designed the study. M.R. performed most of the experiments. T.S. helped to characterize $Myc^{fl/fl}$;FIC/+ mice and to perform the $Malt1^{fl/PM}$;$Foxp3^{eGFP-Cre-ERT2}$ in vivo tamoxifen experiments. T.E. and R.R. generated and bioinformatically analyzed RNA sequencing data. C.W. performed qRT-PCR analyses and helped together with C.M. with the Seahorse assays. C.W. carried out flow cytometry and confocal microscopy on MitoTracker-labeled cells together with T.M. and R.M. M.R. generated the figures. J.R. and M.R. wrote the manuscript. All authors discussed the results and contributed to the manuscript.

## REFERENCES

1 **Nishikawa, H.** and **Sakaguchi, S.**, Regulatory T cells in tumor immunity. *Int. J. Cancer*. 2010. **127**: 759–767.

2 **Tanaka, A.** and **Sakaguchi, S.**, Targeting Treg cells in cancer immunotherapy. *Eur. J. Immunol.* 2019. **49**: 1140–1146.

3 **Vahl, J. C., Drees, C., Heger, K., Heink, S., Fischer, J. C., Nedjic, J., Ohkura, N.** et al., Continuous T cell receptor signals maintain a functional regulatory T cell pool. *Immunity* 2014. **41**: 722–736.

4 **Levine, A. G., Arvey, A., Jin, W.** and **Rudensky, A. Y.**, Continuous requirement for the TCR in regulatory T cell function. *Nat. Immunol.* 2014. **15**: 1070–1078.

5 **Rosenbaum, M., Gewies, A., Pechloff, K., Heuser, C., Engleitner, T., Gehring, T., Hartjes, L.**, et al., Bcl10-controlled Malt1 paracaspase activity is key for the immune suppressive function of regulatory T cells. *Nat. Commun.* 2019. **10**: 2352.

6 **Di Pilato, M., Kim, E. Y., Cadilha, B. L., Prussmann, J. N., Nasrallah, M. N., Seruggia, D., Usmani, S. M.** et al., Targeting the CBM complex causes Treg cells to prime tumours for immune checkpoint therapy. *Nature* 2019. **570**: 112–116.

7 **Cheng, L., Deng, N., Yang, N., Zhao, X.** and **Lin, X.**, Malt1 protease is critical in maintaining function of regulatory T cells and may be a therapeutic target for antitumor immunity. *J. Immunol.* 2019. **202**: 3008–3019.

8 **Yang, D., Zhao, X.** and **Lin, X.**, Bcl10 is required for the development and suppressive function of Foxp3(+) regulatory T cells. *Cell Mol Immunol*. 2021. **18**: 206–218.

9 **Turvey, S. E., Durandy, A., Fischer, A., Fung, S. Y., Geha, R. S., Gewies, A., Giese, T.** et al., The CARD11-BCL10-MALT1 (CBM) signalosome complex: stepping into the limelight of human primary immunodeficiency. *J. Allergy Clin. Immunol.* 2014. **134**: 276–284.

10 **Sun, L., Deng, L., Ea, C. K., Xia, Z. P.** and **Chen, Z. J.**, The TRAF6 ubiquitin ligase and TAK1 kinase mediate IKK activation by BCL10 and MALT1 in T lymphocytes. *Mol. Cell.* 2004. **14**: 289–301.

11 **Ruland, J.** and **Hartjes, L.**, CARD-BCL-10-MALT1 signalling in protective and pathological immunity. *Nat. Rev. Immunol.* 2019. **19**: 118–134.

12 **Monopteros Therapeutics, I.** A study of MPT-0118 in subjects with advanced or metastatic refractory solid tumors. 2023.

13 **Janssen, R.** and **Development, L. L. C.**, A study of JNJ-67856633 in participants With non-Hodgkin's lymphoma (NHL) and chronic lymphocytic leukemia (CLL). 2022.

14 **Jaworski, M.** and **Thome, M.**, The paracaspase MALT1: biological function and potential for therapeutic inhibition. *Cell. Mol. Life Sci.* 2016. **73**: 459–473.

15 **Gewies, A., Gorka, O., Bergmann, H., Pechloff, K., Petermann, F., Jeltsch, K. M., Rudelius, M.** et al., Uncoupling Malt1 threshold function from paracaspase activity results in destructive autoimmune inflammation. *Cell Rep.* 2014. **9**: 1292–1305.

16 **Bornancin, F., Renner, F., Touil, R., Sic, H., Kolb, Y., Touil-Allaoui, I., Rush, J. S.** et al., Deficiency of MALT1 paracaspase activity results in unbalanced regulatory and effector T and B cell responses leading to multiorgan inflammation. *J. Immunol.* 2015. **194**: 3723–3734.

17 **Jaworski, M., Marsland, B. J., Gehrig, J., Held, W., Favre, S., Luther, S. A., Perroud, M.** et al., Malt1 protease inactivation efficiently dampens immune responses but causes spontaneous autoimmunity. *EMBO J.* 2014. **33**: 2765–2781.

18 **Yu, J. W., Hoffman, S., Beal, A. M., Dykon, A., Ringenberg, M. A., Hughes, A. C., Dare, L.** et al., MALT1 protease activity is required for innate and adaptive immune responses. *PLoS One* 2015. **10**: e0127083.

19 **Wing, K., Onishi, Y., Prieto-Martin, P., Yamaguchi, T., Miyara, M., Fehervari, Z., Nomura, T.** et al., CTLA-4 control over Foxp3+ regulatory T cell function. *Science* 2008. **322**: 271–275.

20 **Srinivas, S., Watanabe, T., Lin, C. S., William, C. M., Tanabe, Y., Jessell, T. M.** and **Costantini, F.**, Cre reporter strains produced by targeted insertion of EYFP and ECFP into the ROSA26 locus. *BMC Dev. Biol.* 2001. **1**: 4.

21 **Nagel, D., Spranger, S., Vincendeau, M., Grau, M., Raffegerst, S., Kloo, B., Hlahla, D.** et al., Pharmacologic inhibition of MALT1 protease by phenothiazines as a therapeutic approach for the treatment of aggressive ABC-DLBCL. *Cancer Cell.* 2012. **22**: 825–837.

22 **Johnson, D. G., Schwarz, J. K., Cress, W. D.** and **Nevins, J. R.**, Expression of transcription factor E2F1 induces quiescent cells to enter S phase. *Nature* 1993. **365**: 349–352.

23 **Grumont, R., Lock, P., Mollinari, M., Shannon, F. M., Moore, A.** and **Gerondakis, S.**, The mitogen-induced increase in T cell size involves PKC and NFAT activation of Rel/NF-kappaB-dependent c-Myc expression. *Immunity* 2004. **21**: 19–30.

24 **Grinberg-Bleyer, Y., Oh, H., Desrichard, A., Bhatt, D. M., Caron, R., Chan, T. A., Schmid, R. M.** et al., NF-kappaB c-Rel is crucial for the regulatory T cell immune checkpoint in cancer. *Cell* 2017. **170**: 1096–1108 e1013.

25 **Shono, Y., Tuckett, A. Z., Ouk, S., Liou, H. C., Altan-Bonnet, G., Tsai, J. J., Oyler, J. E.** et al., A small-molecule c-Rel inhibitor reduces alloactivation of T cells without compromising antitumor activity. *Cancer Discov.* 2014. **4**: 578–591.

26 **Wang, W., Tam, W. F., Hughes, C. C., Rath, S.** and **Sen, R.**, c-Rel is a target of pentoxifylline-mediated inhibition of T lymphocyte activation. *Immunity* 1997. **6**: 165–174.

27 **de Alboran, I. M., O'Hagan, R. C., Gartner, F., Malynn, B., Davidson, L., Rickert, R., Rajewsky, K.** et al., Analysis of c-Myc function in normal cells via conditional gene-targeted mutation. *Immunity* 2001. **14**: 45–55.

28 **Saravia, J., Zeng, H., Dhungana, Y., Bastardo Blanco, D., Nguyen, T. M., Chapman, N. M., Wang, Y.** et al., Homeostasis and transitional activation of regulatory T cells require c-Myc. *Sci. Adv.* 2020. **6**, eaaw6443.

29 **Tommasini, A., Ferrari, S., Moratto, D., Badolato, R., Boniotto, M., Pirulli, D., Notarangelo, L. D.** et al., X-chromosome inactivation analysis in a female carrier of FOXP3 mutation. *Clin. Exp. Immunol.* 2002. **130**: 127–130.

30 **Wang, R., Dillon, C. P., Shi, L. Z., Milasta, S., Carter, R., Finkelstein, D., McCormick, L. L.** et al., The transcription factor Myc controls metabolic reprogramming upon T lymphocyte activation. *Immunity*. 2011. **35**: 871–882.

31 **Pourdehnad, M., Truitt, M. L., Siddiqi, I. N., Ducker, G. S., Shokat, K. M.** and **Ruggero, D.**, Myc and mTOR converge on a common node in protein synthesis control that confers synthetic lethality in Myc-driven cancers. *Proc. Natl. Acad. Sci. U. S. A.* 2013. **110**: 11988–11993.

32 **Stine, Z. E., Walton, Z. E., Altman, B. J., Hsieh, A. L.** and **Dang, C. V.**, MYC, metabolism, and cancer. *Cancer Discov.* 2015. **5**: 1024–1039.

33 **Gerriets, V. A., Kishton, R. J., Nichols, A. G., Macintyre, A. N., Inoue, M., Ilkayeva, O., Winter, P. S.** et al., Metabolic programming and PDHK1 control CD4+ T cell subsets and inflammation. *J. Clin. Invest.* 2015. **125**: 194–207.

34 **Chapman, N. M., Zeng, H., Nguyen, T. M., Wang, Y., Vogel, P., Dhungana, Y., Liu, X.** et al., mTOR coordinates transcriptional programs and mitochondrial metabolism of activated Treg subsets to protect tissue homeostasis. *Nat. Commun.* 2018. **9**: 2095.

35 **Angelin, A., Gil-de-Gomez, L., Dahiya, S., Jiao, J., Guo, L., Levine, M. H., Wang, Z.** et al., Foxp3 reprograms T cell metabolism to function in low-glucose, high-lactate environments. *Cell Metab.* 2017. **25**: 1282–1293 e1287.

36 **Goetzman, E. S.** and **Prochownik, E. V.**, The role for Myc in coordinating glycolysis, oxidative phosphorylation, glutaminolysis, and fatty acid metabolism in normal and neoplastic tissues. *Front Endocrinol (Lausanne)*. 2018. **9**: 129.

37 **Huang, M. J.**, **Cheng, Y. C.**, **Liu, C. R.**, **Lin, S.** and **Liu, H. E.**, A small-molecule c-Myc inhibitor, 10058-F4, induces cell-cycle arrest, apoptosis, and myeloid differentiation of human acute myeloid leukemia. *Exp. Hematol.* 2006. **34**: 1480–1489.

38 **Graves, J. A.**, **Wang, Y.**, **Sims-Lucas, S.**, **Cherok, E.**, **Rothermund, K.**, **Branca, M. F.**, **Elster, J.** et al., Mitochondrial structure, function and dynamics are temporally controlled by c-Myc. *PLoS One* 2012. **7**: e37699.

39 **Edmunds, L. R.**, **Sharma, L.**, **Wang, H.**, **Kang, A.**, **d'Souza, S.**, **Lu, J.**, **McLaughlin, M.** et al., c-Myc and AMPK control cellular energy levels by cooperatively regulating mitochondrial structure and function. *PLoS One* 2015. **10**: e0134049.

40 **Morrish, F.** and **Hockenbery, D.**, MYC and mitochondrial biogenesis. *Cold Spring Harb. Perspect. Med.* 2014. **4**: a014225.

41 **Dai, B.**, **Grau, M.**, **Juilland, M.**, **Klener, P.**, **Horing, E.**, **Molinsky, J.**, **Schimmack, G.** et al., B-cell receptor-driven MALT1 activity regulates MYC signaling in mantle cell lymphoma. *Blood.* 2017. **129**: 333–346.

42 **Rubtsov, Y. P.**, **Niec, R. E.**, **Josefowicz, S.**, **Li, L.**, **Darce, J.**, **Mathis, D.**, **Benoist, C.** et al., Stability of the regulatory T cell lineage in vivo. *Science.* 2010. **329**: 1667–1671.

43 **Parekh, S.**, **Ziegenhain, C.**, **Vieth, B.**, **Enard, W.** and **Hellmann, I.**, The impact of amplification on differential expression analyses by RNA-seq. *Sci. Rep.* 2016. **6**: 25533.

44 **Macosko, E. Z.**, **Basu, A.**, **Satija, R.**, **Nemesh, J.**, **Shekhar, K.**, **Goldman, M.**, **Tirosh, I.** et al., Highly parallel genome-wide expression profiling of individual cells using nanoliter droplets. *Cell* 2015. **161**: 1202–1214.

45 **Core Team R**, *R: A language and environment for statistical computing*. R Foundation for Statistical Computing, Vienna, Austria 2014.

46 **Love, M. I.**, **Huber, W.** and **Anders, S.**, Moderated estimation of fold change and dispersion for RNA-seq data with DESeq2. *Genome Biol.* 2014. **15**: 550.

47 **Ritchie, M. E.**, **Phipson, B.**, **Wu, D.**, **Hu, Y.**, **Law, C. W.**, **Shi, W.** and **Smyth, G. K.**, limma powers differential expression analyses for RNA-sequencing and microarray studies. *Nucleic. Acids. Res.* 2015. **43**: e47.

48 **Subramanian, A.**, **Tamayo, P.**, **Mootha, V. K.**, **Mukherjee, S.**, **Ebert, B. L.**, **Gillette, M. A.**, **Paulovich, A.** et al., Gene set enrichment analysis: a knowledge-based approach for interpreting genome-wide expression profiles. *Proc. Natl. Acad. Sci. U. S. A.* 2005. **102**: 15545–15550.

49 **Cossarizza, A.**, **Chang, H. D.**, **Radbruch, A.**, **Acs, A.**, **Adam, D.**, **Adam-Klages, S.**, **Agace, W. W.** et al., Guidelines for the use of flow cytometry and cell sorting in immunological studies (second edition). *Eur. J. Immunol.* 2019. **49**: 1457–1973.

*Abbreviations:* **MALT1i**: MALT1 inhibitor · **rTregs**: resting Tregs · **Tconv**: conventional T · **UMIs**: Unique Molecular Identifiers

*Full correspondence:* Dr. Jürgen Ruland, Institute of Clinical Chemistry and Pathobiochemistry, School of Medicine, Technical University of Munich, 81675 Munich, Germany
e-mail: j.ruland@tum.de